PAPER

Check for updates

A simple, sustainable route to flexible microporous carbon cloth for energy storage applications†

Thria Alkhaldi, [ID] [ab] L. Scott Blankenship [ID] [a] and Robert Mokaya [ID] *[a]

Activated carbon cloth (ACC) has the potential to be extremely useful in gas capture and storage applications as it combines high porosity, robustness, and flexibility with ease of handling. While it has been produced by a few researchers, the synthesis methods used to date either do not yield a product with high porosity, or if appropriate textural properties are achieved the synthesis is complex and arduous. Following a systematic study, we show that an almost exclusively microporous flexible ACC can be achieved with surface area >1900 m^2 g^{-1} *via* stabilisation with NH_4Cl only, followed by activation with benign activating agent potassium oxalate (PO). After extensive optimisation and simplification of the process, it was found that the stabilisation step can be omitted in a synthesis route requiring only a simple carbonisation step to produce a flexible microporous carbon with surface area >2200 m^2 g^{-1}, thus further reducing the need for additional solvents and reagents. The CO_2 and CH_4 uptake of the ACCs developed in this work is comparable to that previously reported for flexible porous carbons prepared *via* more complicated routes and the porosity of the ACCs can be tuned to specific gas uptake applications according to the synthesis conditions.

1 Introduction

Activated carbons are widely employed as effective adsorbent materials for the storage of adsorbates such as H_2, CH_4, and CO_2 due to their large specific surface areas (SSA), good chemical stability and low cost. When nanoporous activated carbon is used for these applications, it must still be treated to generate a functional material (*e.g.*, membranes, thin films) from carbon powder. This results in a lowering of the specific surface area and specific pore volume, due to the effects of aggregation and pore blockage.[1] Since these textural properties play a key role in energy storage applications, it would be highly desirable to develop a cost-effective and simple processing procedure for a lightweight, mechanically and chemically stable, flexible, non-fragile material without losing porosity. This may exist in the form of activated carbon cloth (ACC),[2,3] whose conformability and flexibility make it much more

versatile and robust as a potential liner in gas storage tanks. Recently, ACCs have been suggested as such a flexible form of activated carbon that may function as an efficient gas adsorbent. In the case of use as absorbents for energy related gases (*e.g.*, CO_2, CH_4 and H_2), such flexible activated carbon cloth would be much easier to handle than powder and granular forms. They would offer the processability and mechanical properties required for the construction of more efficient storage tank designs incorporating the carbons as coatings or liners inside tanks. In addition a continuous material like carbon cloth does not have interparticle voids which are present in powders. Adsorption of small molecules is associated mainly with micropores and narrow mesopores, thus the porosity attributed to these larger interparticle voids is not particularly useful in this type of application.[4–10] Thus ACCs may provide a method to maximising 'useful' porosity.

With respect to possible precursors for ACCs, previous work has inspired by reported syntheses of the related material, carbon fibre (CF).[11,12] While both polyacrylonitrile and cellulose-based materials have been used,[13–16] the latter are today favoured for their lower production cost and the fact that they do not derive from fossil fuels.[11,17] In particular, synthetic textiles are more suitable than natural cellulosic fibres due to due to their structural regularity as well as lack of impurities (especially lignin and hemicellulose) which can result in low yield and poor porosity in derived materials.[11,18,19] As such the regenerated cellulosic

^{a} *School of Chemistry, University of Nottingham, University Park, Nottingham, NG7 2RD, UK. E-mail: r.mokaya@nottingham.ac.uk*

^{b} *Department of Chemistry, Jeddah University, Jeddah 23442, Saudi Arabia*

† Electronic supplementary information (ESI) available: One PDF file with all referenced supporting information, as well as isotherms in.aif format, and a pyhton module for the calculation of total adsorption from excess available at https://github.com/sblanky/total_adsorption. See DOI: https://doi.org/10.1039/d3ma00157a
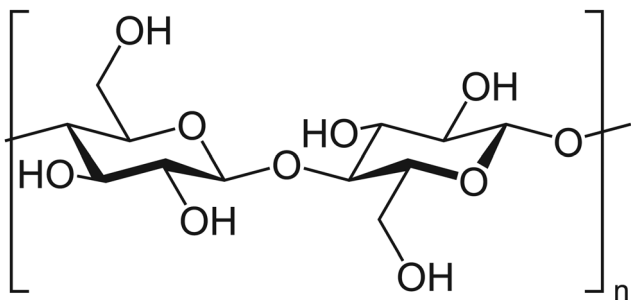
Fig. 1 The structure of cellulose, of which VR fibres are composed.[22]

(structure shown in Fig. 1) fibre, viscose rayon (VR) has become the precursor of choice in ACC synthesis.[11,12,20,21]

Preparation of ACC from VR has been attempted by a number of methods.[2,3,20,21,23–25] The principal hurdle is to facilitate development of porosity and removal of heteroatoms (principally O) via carbonisation from the original textile, without impinging on the structural integrity of the material at the macro scale. As such, some researchers have favoured pyrolysis of VR following impregnation with reagents such as chloride and phosphate salts in order to promote porogenesis via dehydration reactions[4,26,27] over the depolymerisation that occurs on thermal treatment of textiles.[2,3,23,28] When successful, these reagents can be simultaneously considered stabilisers and porogens. Huidoboro et al. found that pore size could be tuned in these processes by selection of the appropriate dehydrating agent; reagents such as $ZnCl_2$ and H_3PO_4 promote micropore formation, whereas ACCs derived via impregnation with Na_2HPO_4 resulted in principally mesoporous products.[3] Due to the low porosity of these ACCs (maximum reported surface area, A_{BET} is 643 m^2 g^{-1})[23] Kostoglou et al. used physical activation with CO_2 to produce a microporous ACC with surface area of over 1200 m^2 g^{-1} from VR impregnated with $ZnCl_2$ and NH_4Cl.[21] As is typical for activation with CO_2[4,29] this unfortunately came at the cost of a very high pyrolysis temperature of 930 °C. On the other hand, activation of biomass with KOH has been found to reliably produce activated carbon powder with ultrahigh porosity,[1,4,30,31] thus Attia and co-workers used this technique to produce ACCs from a stabilised textile with surface area and pore volume over 1900 m^2 g^{-1} and 0.80 mL g^{-1} respectively. However, prior to stabilisation with $ZnCl_2$ and NH_4Cl, the surface of the VR was decorated with polypyrrole nanoparticles.[20] It is therefore unclear whether the improvements in the porosity of the resulting ACC are a result of activation of the polypyrrole or the VR itself, as the former has been successfully used to produce highly porous activated carbons.[32]

As described above, the current state-of-the-art methods for preparing cellulose-based ACCs involve a number of steps that consume significant energy, chemicals and time. Sustainable, efficient syntheses are achievable by (among other factors) the minimisation of the number of reagents and the number of steps used. Thus far, moderate to highly porous ACC has only been produced from VR in two or more steps, i.e. (i) impregnation

with $ZnCl_2$ and NH_4Cl and (ii) activation with either CO_2 or KOH.[20,21] Therefore, this work details attempts at simplifying and improving the sustainability of the synthesis of ACC, via three broad methods; (i) omitting the stabilisation step, i.e. negating the use of $ZnCl_2$ and NH_4Cl which has to date been considered to be a crucial step in the preparation of ACCs that preserve the flexibility of activated carbon fabric, (ii) not using an additional activating agent, and (iii) use of the less caustic activating agent potassium oxalate (PO), which has previously been shown to give comparable porosity in activated carbons to the more commonly used KOH.[33–35] Due to porosity of the resulting ACCs and the sparsity of the literature on the gas uptake capacity of ACCs in general, we explored the CO_2 and CH_4 uptake of the materials prepared in this work.

2 Experimental

Dyed viscose rayon (VR) with a 2/2 twill weave was obtained from a local fabric shop.

2.1 Synthesis

Synthesis of ACC was performed via five methods, each starting with a piece of VR (7 × 7 cm). The titles of subsections below reflect the pre-treatment of VR prior to thermal treatment (i.e. activation). In all cases, activation was attempted by heating the sample in a tube furnace under N_2 (60 mL min^{-1}) at some temperature for 1 h. Ramp rate to the target temperature was 5 °C min^{-1}. In order to remove any contaminants left by the porogen(s), all samples were subsequently washed by stirring in aqueous HCl solution (400 mL, 10 vol%) for 2 h, then rinsed with sufficient deionised water to give neutral washings. Washed material was then dried overnight at 100 °C.

2.1.1 Direct activation. VR was soaked in aqueous KOH solution (0.2 M, 100 mL) for 1 h, then dried to remove excess water at 60 °C for 30 min. Activation occurred at 650 °C and the resulting sample is denoted VRd, where d indicates direct activation.

2.1.2 Stabilisation. Activation with KOH was attempted of VR that had been structurally stabilised by being first immersed for 1 h in 100 mL of an aqueous solution of NH_4Cl and $ZnCl_2$ (1.5 g (0.28 M) and 1.8 g (0.13 M), respectively) and then dried at 60 °C for 1 h. The stabilised VR was then soaked in 100 mL of 0.2 M KOH solution for 5 min and dried at 60 °C for 30 min as previously, then activated at 700 °C for 1 h following a ramp rate of 5 °C min^{-1}. Following washing and drying as above, the resulting sample was denoted VRnzK-700, with n and z indicating stabilisation with NH_4Cl and $ZnCl_2$ respectively, K activation with KOH, and 700 indicating activation at 700 °C.

Cognisant that $ZnCl_2$ has been extensively exploited as an activating agent (porogen),[23,26,27,36,37] the above procedure was modified such that the stabilised VR was activated without the use of KOH. The concentration of the $NH_4Cl/ZnCl_2$ solution was varied by changing the volume of water used (100, 50 or 10 mL) and activation was carried out at 630 or 700 °C following a ramp rate of 5 °C min^{-1}. Following washing and drying as above,

samples derived *via* this method were designated VRnzZ-*X*-*T*, where the (capital) Z indicates that ZnCl$_2$ also takes the role of an activating agent and *X* and *T* indicate the volume of stabilising solution and activation temperature respectively. Thus, a sample prepared using 50 mL of NH$_4$Cl/ZnCl$_2$ solution at 700 °C is designated as VRnzZ-50-700.

In a further modification of the synthesis route, potassium oxalate (PO) was investigated as an alternative activating agent. Stabilisation of VR was performed by immersion in 10 mL of an aqueous solution of 0.28 M NH$_4$Cl for 1 h at room temperature, and then drying at 60 °C. The NH$_4$Cl-stabilised VR was soaked in 1.2 M PO solution and then dried at 60 °C for 30 min. Activation of the NH$_4$Cl-stabilised VR/PO mixture was then performed at 750, 800 or 900 °C for 1 h following a ramp rate of 5 °C min^{-1}. Following washing and drying as described above, the resulting samples were designated VRnP-*T*, where n signifies stabilisation with NH$_4$Cl, P indicates activation with potassium oxalate and *T* is the activation temperature. Thus a sample activated at 800 °C is designated as VRnP-800.

2.1.3 Carbonisation. Finally, preparation of flexible ACC was attempted *via* activation with PO without using stabilising reagents. Prior to activation, the VR was carbonised under a flow of N$_2$ (60 mL min^{-1}) at 800 °C for 1 h following a ramp rate of 5 °C min^{-1}. The carbonised VR was designated VRc with c indicating carbonisation. The VRc was then impregnated with PO as described above (*i.e.* soaked in 1.2 M aqueous PO solution then dried at 60 °C for 30 min). The VRc/PO mixture was then activated at 650, 700, 750, 800 or 900 °C. Following washing and drying as described above, these samples are denoted VRcP-*T* where P indicates PO activation and *T* is the activation temperature. Thus a sample activated at 800 °C is designated as VRcP-800.

2.2 Material characterisation

CHN elemental analysis was performed on a CE440 Elemental Analyser (Exeter Analytical). For assessment of sample graphititic nature and identification of any crystalline materials, XRD measurements were taken on a PANalytical X'Pet Pro diffractometer using CuKα X-rays (40k, 40 m) with a wavelength of 1.5418 Å, at 2θ between 2 to 80°. Angular and time step size between scans were 0.02° and 50 s respectively. SEM images were collected on a JEOL JSM-7100F with an accelerating voltage of 5 kV.

To assess porosity, N$_2$ (Air products, technical grade) sorption isotherms were measured at −196 °C on a Micrometics 3flex sorptometer. Isotherm measurement was in the relative pressure range 1 × 10^{-8} to 1, with P_o determined by the pressure of liquid N$_2$ in the reference tube. Up to relative pressure of 4 × 10^{-4} the equilibration interval was 45 s; full details of the analysis procedure are available in the ESI,† Table S1. Following isotherm measurement, freespace (void volume) was measured using He (Air products, technical grade) at both ambient and anlysis temperature. Prior to analysis, the carbon samples were degassed on a Micromeritics Smart VacPrep under vacuum (at least 1 × 10^{-4} mbar). After vaccuum was achieved, samples were then heated at 10 °C min^{-1} to 90 °C

for 1 h, then ramped at 10 °C min^{-1} to 200 °C and held for 12 h, before being allowed to cool under vaccum. Sample tubes were then backfilled with N$_2$ prior to transferring to the sorptometer. On the analysis port, samples were again degassed for 1 h at a vacuum of at least 1 × 10^{-5} at ambient temperature, and 1 × 10^{-8} at cryogenic temperature.

From the isotherms, surface area (A_{BET}) was determined using the Rouquerol criteria[38] *via* the BETSI method so as to improve reproducibility.[39] Further details of the method as well as the results can be found in the ESI† Section S6, including graphical outputs showing the relative pressure range used for each isotherm and filter parameters used. Total pore volume was determined using the single point method on the isothermal plateau (relative pressure ∼0.9), and micropore volume and micropore surface area were calculated with the t-plot method using the carbon black STSA thickness curve. Pore size distributions (PSDs) were calculated using the SAIEUS software and the 2D-NLDFT heterogeneous surface kernel with a fitting parameter, λ of 3.5 for all isotherms.[40,41] This kernel was used as it accounts for the chemical heterogeneity present in ACs and ACCs. Further details can be found in the ESI,† Section S7 alongside a graphical display of the fits. Values of overall porosity, *i.e.* A_{NLDFT} and V_{NLDFT} can then be extracted from cumulative PSDs as well as porosity within some range of pore widths; *i.e.* micro-, ultramicroporosity *etc.*

2.3 Gas uptake measurements

Gravimetric gas uptake isotherms were measured at 25.00 ± 0.01 °C controlled by a constant temperature, flowing water bath on a XEMIS gravimetric sorption analyser (Hiden). Sample masses were at least 50 mg, and the mass measurement precision of XEMIS is 0.1 μg with a mass stability of 1 μg. CO$_2$ (Air products, Industrial grade) and CH$_4$ (BOC, purity 99.9995%) isotherms were measured up to 40 and 100 bar respectively. The pressure precision for any isotherm point is 0.02% at any point, and the base vaccuum pessure is < 1 × 10^{-6} mbar. Equilibrium uptake was determined by identifying the asymptote of rate of change in uptake after a relaxation of 99% (tolerance 2%). Data was sampled at an interval of 1 s. Prior to isotherm measurement, samples were degassed insitu at 240 °C (ramp rate 10 °C min^{-1}) for at least 4 h until sample mass was stable.

Measurements on the XEMIS give excess uptakes, *i.e.* the uptake of gas above that which would have been taken up in a volume equivalent to that of the total pore volume at the same pressure and temperature but without the attractive interactions between gas molecules and pore walls of the adsorbate. This requires skeletal density, which was mesured using He pycnometry on a Micromertics Accupyc II. For CH$_4$ storage studies, total (absolute) quantity adsorbed, Q_t is a more practical measure. The total mass adsorbed (m_t) may be estimated from the excess mass of CH$_4$ adsorbed by 1 g of adsorbent, m_{exc} (g) from eqn (1);[42,43]

$$m_t = m_{exc} + d_{CH_4}V_t \qquad (1)$$

where d_{CH_4} is the bulk density of CH$_4$ at the pressure and temperature of the isothermal point, and V_t is the pore volume
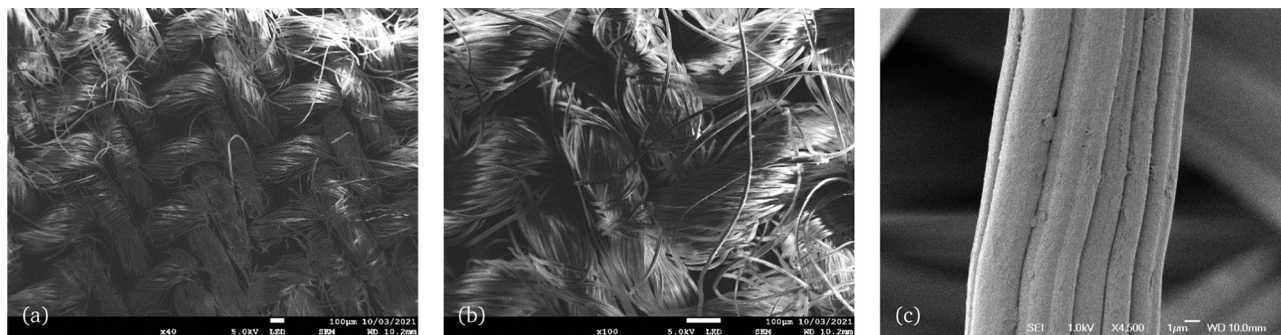
Fig. 2 SEM images of VR taken at magnification of (a) × 40, (b) × 100, and (c) × 4500.

of the sample, which for the purposes of this study was the single point pore volume V_{sp}.‡ d_{CH_4} was determined using the PropsSI function in the CoolProp library.[44] From m_t the determination of the molar quantity adsorbed, Q_t (mmol g^{-1}) is trivial. These calculations were automated with a short python script which is available on **github**.

3 Results and discussion

Elemental analysis of VR indicated C and H content of 40 and 6 wt%. O content can thus be assumed to be 54 wt%. As shown in Fig. 2(a), VR is made of woven fibres that are relatively continuous (Fig. 2(c)). This general structural continuity exhibited in the textile must be maintained in the activated products in order to retain flexibility.

3.1 KOH-activation

The direct activation of VR with KOH resulted in the product, VRd being entirely powder activated carbon. The C-content of VRd was 72 wt% (*cf.* 41 wt% for VR) while the O- and H- content were reduced from 53 to 26 wt% and 6 to 1 wt% respectively. Regarding porosity, VRd exhibited a fully reversible nitrogen sorption isotherm with type I characteristics (see Fig. S28, ESI†) indicating that the carbon was mainly microporous. The pore size distribution curve of VRd indicates the presence of micropores (Fig. S28, ESI†). VRd had a surface area of 944 m^2 g^{-1} with 80% (753 m^2 g^{-1}) arising from micropores. This process highlighted the fact that KOH-activation was overly harsh, and therefore not a suitable choice as an activating agent for the direct preparation of flexible ACC.

In the next synthesis attempt, VR was first stabilised with NH_4Cl and $ZnCl_2$ prior to KOH activation. The stabilisation gave gave more encouraging results; flexibility of the precursor was retained after stabilisation, and the resultant product (VRnzK-700) retained flexibility in some areas of the cloth following activation with KOH, however significant portions of the cloth hardened (Fig. S2, ESI†). This indicates that the flexibility of the similar material created by Attia *et al.* using a

‡ V_t - derived using porosimetry - is used as an estimate for V_{ads}, the adsorbed volume of CH_4, in the absence of a preferable method.

Table 1 Elemental compositon (wt%) of VR and products derived *via* activation with KOH either directly to powdered VRd or following stabilisation to partially flexible and powdered (hard) VRnzK-700

Sample	C	H	N	O
VR	41	6.0	0.0	54
VRd	72	1.0	0.0	26
VRnzK-700 (hard)	56	0.5	0.0	44
VRnzK-700 (flexible)	69	1.6	5.8	24

similar stabilisation procedure but with the inclusion of polypyrrole nanoparticles can be at least partially attributed to the polypyrrole.[20] It should be noted that, as shown in Table 1, the flexible portion of VRnzK-700 has significantly higher C, (69 *vs.* 56 wt%) as well as N (5.8 wt% *vs.* nil) content compared to the hard (powdered) portion. This indicates adsorption of NH_4Cl into at least some regions of the precursor, resulting in the evident partial stabilisation. The powder and flexible portions of VRnzK-700 have nitrogen sorption isotherms of similar shape (see Fig. S28, ESI†), but the former has higher surface area; 1263 *vs.* 847 m^2 g^{-1}, and pore volume 0.8 *vs.* 0.6 cm^3 g^{-1}. Although both parts have comparable pore size distributions (Fig. S28, ESI†), the powder form has higher levels of microporosity at 85 *vs.* 75% for surface area (*i.e.*, 1076 *cf.* 647 m^2 g^{-1}) and 63 *vs.* 50% for pore volume (*i.e.* 0.5 *cf.* 0.3 cm^3 g^{-1}). The relatively low content of C in both portions of VRnzK-700 relative to VRd indicates that some part of the stabilisation procedure may prevent the degradation of volatile oxygen rich moieties during activation/pyrolysis. Further data for VRd and VRnzK-700 can be found in the ESI† (Fig. S5, S6, S28 and Table S2), but the remainder of this work discusses the flexible products. It is clear that KOH is not the best candidate for activation of VR to flexible ACC, even with the presence of stabilising reagents. The corrosive nature of KOH clearly limits the stabilising effects of NH_4Cl and $ZnCl_2$, thus a gentler activation strategy is required.

3.2 Flexible ACCs

The three remaining routes, *i.e.* stabilisation of VR with NH_4Cl and $ZnCl_2$ followed by thermal treatment to facilitate activation with the latter ($ZnCl_2$) rather than using KOH (Fig. S3, ESI†); stabilisation of VR with NH_4Cl only followed by activation with

Table 2 Elemental compositon (wt%) of flexible ACCs (series VRznZ-*X-T*) derived from VR using $ZnCl_2$ as the sole activating agent

Sample	C	H	N	O
VRnzZ-10-630	58	1.5	6.8	34
VRnzZ-50-630	60	1.6	6.1	32
VRnzZ-100-630	81	1.6	4.3	14
VRnzZ-10-700	69	1.5	5.8	24
VRnzZ-50-700	74	0.5	3.8	21

Table 3 Elemental composition (wt%) of flexible ACCs derived using from VR using PO as an activating agent following stabilisation with NH_4Cl only (VRnP-*T*) or following carbonisation only (VRcP-*T*). The data for carbonised VR (VRc) is also shown

Sample	C	H	N	O
VRnP-750	76	0.1	0.0	24
VRnP-800	82	0.9	0.3	17
VRnP-900	84	1.0	0.5	15
VRc	85	0.5	0.2	15
VRcP-650	82	0.3	0.4	17
VRcP-700	83	0.3	0.3	17
VRcP-750	90	0.0	0.1	10
VRcP-800	87	0.3	0.3	12
VRcP-900	82	0.2	0.3	18

PO (Fig. S4, ESI†); and carbonisation followed by PO activation (series VRcP-*T*) all resulted in fully flexible ACC regardless of changes in activation temperature, concentration of stabilising solution, and/or amount of porogen (where applicable).

3.2.1 Composition and carbon nature. The composition of the flexible ACCs is shown in Tables 2 and 3. Parallels can be drawn between the composition of the $ZnCl_2$-activated samples (VRnzZ-*X-T*, Table 2) and the KOH activated sample VRnzK (see Table 1). Firstly, similar to flexible VRnzK-700, the VRnzZ-*X-T* samples exhibit a relatively high N content of between 3.8 and 6.8 wt% which is a result of impregnation with NH_4Cl. However, the concentration of the NH_4Cl/$ZnCl_2$ stabilising/porogen solution does not appear to particularly correspond to final N content. Washing with HCl evidently removes any vestigial Zn and Cl according to TGA and P-XRD analysis (Fig. S5 and S6, ESI†), but N is retained. This may indicate that over the course of stabilisation and activation, N becomes bonded to the evolving carbonaceous structure in a manner similar to that for intentional synthesis of N-doped carbons.[31,45–47] In a further parallel to the VRnzK-700 sample, the C content for the VRnzZ-*X-T* samples remains relatively low (<70 wt%) at both low activation temperature (630 °C), and at low dilution of stabilising solution (10 or 50 mL). This indicates that, as hoped, the promotion of dehydration reactions partially overcomes the degradation of labile parts of the cellulosic VR structure during the thermal activation step. However, for sufficiently high dilutions of stabiliser (100 mL) and/or high enough activation temperature (samples VRnzZ-100-630 and VRnzZ-50-700) a C-rich (up to 81 wt%) product can be obtained. Fortunately, this loss of N heteroatoms does not appear to compromise the ACC's flexibility, suggesting that retention of heteroatoms may not be essential for attaining a flexible product.

On the other hand, use of PO as activating agent appears to almost completely eliminate any N from ACCs derived from NH_4Cl-stabilised VR (series VRnP-*T*, see Table 3). The N content for some VRnP-*T* samples is above nil, but this is also the case for the samples derived without NH_4Cl (VRc and VRcP-*T*) so this very low N content can be ascribed to small amounts of contamination. The loss of N must then be attributed to reactions between NH_4Cl and PO, possibly forming salts of cyanide and/or cyanate as has been observed previously for pyrolytic reactions involving metal salts and N-enrich precursor mixtures.[48,49] As should be expected, the C/O ratio can be increased for these samples simply by increasing the activation temperature. The C content and consequently the C/O ratio can be increased for flexible ACCs simply by increasing the activation temperature.

Direct pyrolysis at 800 °C of VR to yield VRc more than doubles the C content to 85 wt% (Table 3), which is also slightly higher than that for all of the NH_4Cl-stabilised, PO-activated ACCs (series VRnP-*T*). This is because the degradative depolymerisation reactions taking place on heating naked VR are not competing with reactions arising from to the presence of stabiliser or, indeed an activating agent. However on activation of VRc with PO, the relationship between C/O ratio and activation temperature is somewhat more complex. Firstly, activation at 650 and 700 °C results in a lower C content than that of VRc. A similar trend has previously been reported for the PO-activation at 600 °C of a highly carbon rich precursor.[50] On the other hand, for activation at 750 and 800 °C, the C content increases up to 90 wt% which is more than that of both VRc and the equivalent NH_4Cl-stabilised ACCs which are activated at the same temperatures. VRcP-900 however has a C content of only 82 wt% which is lower than that of both VRc and VRnP-900. As such, it can be inferred that PO does not solely have an oxidative effect, *i.e.* the production of K_2CO_3 on reactions with C which is subsequently removed during washing. Indeed at both low and high temperatures, activation of VRc with PO appears to result in the incorporation of O-rich moieties into the structure of the resultant ACC. While it is common for C content to plateau at high activation temperatures using K-salt porogens including PO,[35,50,51] to our knowledge this decrease in C at high temperatures has thus far only been reported for some carbons derived from cellulose acetate.[30]

XRD analysis of the flexible ACCs (Fig. S5, ESI†) confirmed the absence of any retained inorganic matter as there were no sharp peaks indicative of crystalline material. This confirms that the washing step is effective in ensuring that the ACCs are purely carbonaceous. This is confirmed by TGA - see Fig. S6 (ESI†). Regarding the nature of the carbon cloths, the XRD patterns of VRnzZ-*X-T* samples (Fig. S5, ESI†) show broad peaks at 2ϑ of 23 and 43° which correspond to the (002) and (100) reflections of turbostratic carbon. The broad nature of the peaks indicates that the carbon cloths are essentially amorphous rather than graphitic, which is consistent with what is expected for activated carbons. The XRD patterns of the PO-activated VRnP-*T* and VRcP-*T* series of flexible ACCs (Fig. S7b and c, ESI†) indicate that they are also essentially amorphous

with very low levels of graphitisation. The ACCs prepared at a low activation temperature (750 °C) appear to have a comparatively higher of graphitisation, which is consistent with higher temperatures disrupting any graphitic domains that may be present.

3.3 Morphology

Exemplar SEM images of the flexible ACCs can be found in Fig. 3 (and Fig. S7–S10, ESI†). In general, the fibrous structure of the original VR (Fig. 2) can still be seen, which explains the fact that the products remain flexible. However the morphology and integrity of the fibers is disrupted. The extent of the disruption may relate to both the harshness of activation conditions and/or which porogens/stabilisers were used in the synthesis. Some breakage of fibers is evident for ACCs that were derived using stabilising reagents observed in Fig. 3 for

sample VRnzZ-10-700 and VRnP-900. This is also evident for other ACCs in series VRnzZ-*X-T* (Fig. S7, ESI†) and VRnP-*T* (Fig. S8, ESI†) though the disruption appears to be more extensive for the former. Apart from this, there is clear evidence of the formation of grooves and holes in the fibres in the case of VRnzZ-*X-T* samples as shown in Fig. 3 and Fig. S9 (ESI†) which is not seen for series VRnP-*T* (Fig. 3 (middle row) and Fig. S7, ESI†). This indicates that the use of $ZnCl_2$ as a porogen results in some etching of the fibres, however etching (at least that which is visible with SEM) does not seem to occur for activation with PO. The extent of the etching and/or breakage does appear to be related to the dilution, *X*, of the $NH_4Cl/ZnCl_2$ solution used in the synthesis of VRnzZ-*X-T*. This can be discerned by comparing the morphology of samples synthesised with a total stabilising solution volume of 50 and 10 mL (see Fig. 3 and Fig. S7–S10, ESI†) where the higher concentration in the latter
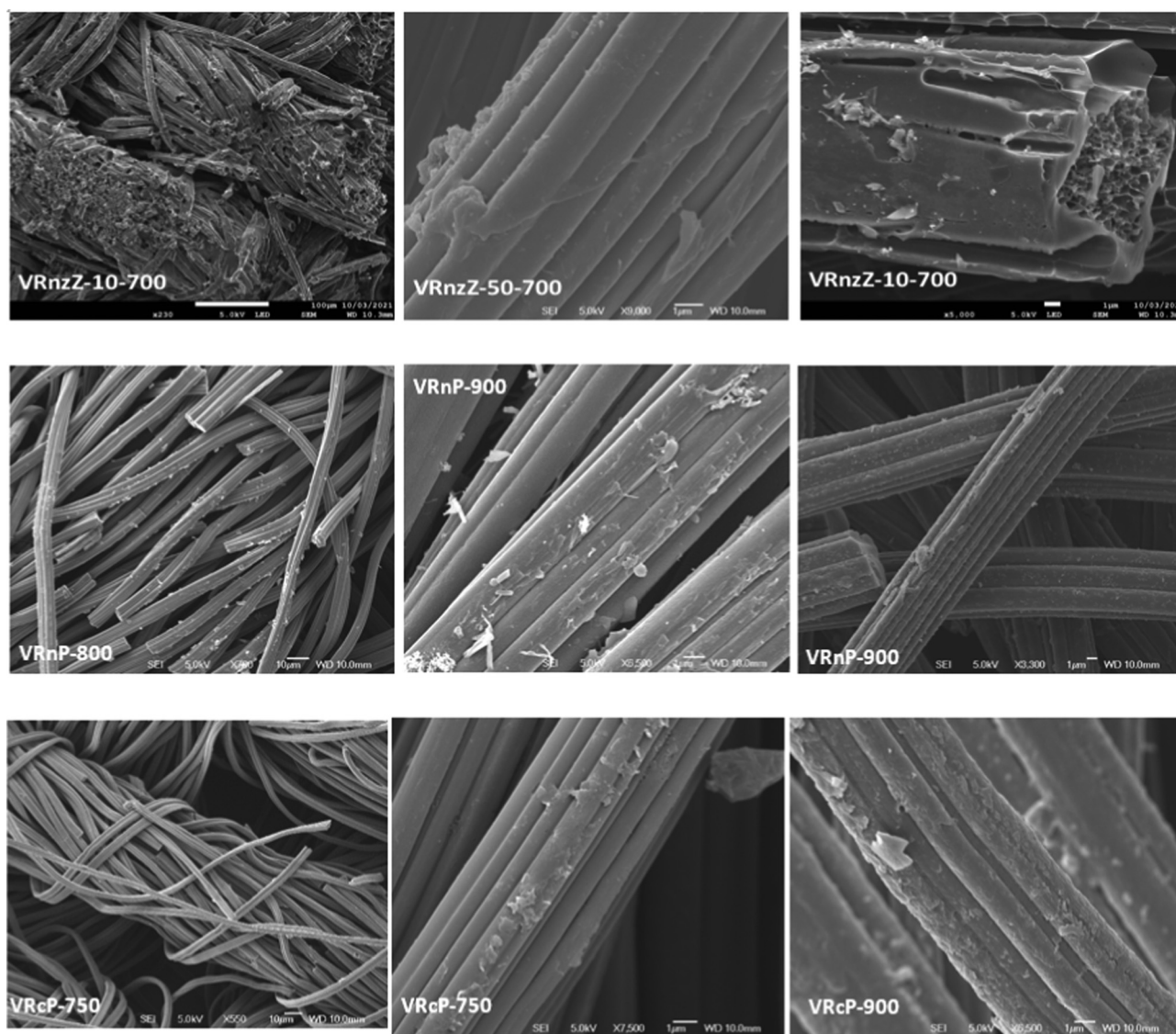

Fig. 3 SEM images of the three series of flexible ACCs selected to show effects of the synthesis regime and harshness of activation on the fibrous structure; VRnzZ-*X-T* (top row), VRnP-*T* (middle row), and VRcP-*T* (bottom row).

Table 4 Measures of porosity of flexible ACCs. Classical measures (A_{BET}, V_{sp}) are accompanied by that proportion taken up by micropores as an absolute value and a percentage of the total. Surface area density, SAD is calculated as the ratio of A_{BET} to V_{sp}. For NLDFT-derived measures (A_{NLDFT}, V_{NLDFT}) the bracketed numbers are indicative of porosity below 10 Å. See the ESI, Sections S6 and S7 for further information on the A_{BET} and PSD calculations respectively

Sample	A_{BET}/m^2 g^{-1}		V_{sp}/cm^3 g^{-1}		SAD/m^2 cm^{-3}	A_{NLDFT}/m^2 g^{-1}		V_{NLDFT}/cm^3 g^{-1}	
VRnzZ-10-630	947	(909, 96%)	0.39	(0.35, 91%)	2460	819	(737, 90%)	0.36	(0.30, 82%)
VRnzZ-50-630	1222	(1208, 99%)	0.47	(0.47, 99%)	2600	1051	(968, 98%)	0.44	(0.40, 90%)
VRnzZ-100-630	926	(883, 95%)	0.40	(0.36, 90%)	2344	1157	(1152, 100%)	0.38	(0.36, 95%)
VRnzZ-10-700	598	(581, 97%)	0.24	(0.23, 95%)	2471	854	(852, 100%)	0.25	(0.24, 97%)
VRnzZ-50-700	965	(893, 93%)	0.41	(0.35, 84%)	2354	1232	(1174, 95%)	0.42	(0.34, 82%)
VRnP-750	1933	(1841, 95%)	0.80	(0.72, 90%)	2416	1735	(1601, 92%)	0.77	(0.62, 81%)
VRnP-800	993	(963, 97%)	0.40	(0.37, 93%)	2489	1148	(1117, 97%)	0.38	(0.35, 92%)
VRnP-900	1095	(1058, 97%)	0.45	(0.41, 93%)	2455	1125	(1037, 92%)	0.44	(0.35, 81%)
VRcP-650	942	(876, 93%)	0.42	(0.36, 86%)	2243	1159	(1044, 90%)	0.43	(0.32, 74%)
VRcP-700	1013	(966, 95%)	0.44	(0.40, 91%)	2302	1233	(1098, 89%)	0.45	(0.33, 74%)
VRcP-750	2226	(1803, 81%)	1.26	(0.80, 63%)	1767	2105	(1452, 69%)	1.17	(0.50, 43%)
VRcP-800	713	(657, 92%)	0.30	(0.26, 87%)	2377	830	(767, 92%)	0.31	(0.24, 77%)
VRcP-900	701	(663, 95%)	0.29	(0.26, 90%)	2417	816	(789, 97%)	0.29	(0.25, 87%)

caused greater etching and breakage of the fibres. Finally, for all synthesis routes activation temperature alone does not appear to have a great effect on the structure of the derived samples.

Samples derived *via* the sequential carbonisation and PO activation of VR appear to suffer only limited breakage of the fibres, or only small amounts of etching of the surface as shown in Fig. 3 for VRcP-750 and VRcP-900, and which is indeed the case for all VRcP-*T* samples (Fig. S10, ESI†). There is, however, some mild deformation relative to the pristine VR fibres (*cf.* Fig. 2 and Fig. 3 (bottom row) and Fig. S10, ESI†). This indicates that the two heating stages were mild and did not cause extensive damage to the VR fibres unlike what is observed with use of the so-called 'stabilising' reagents, especially ZnCl$_2$. This further confirms the relative gentleness/mildness of activation with PO with respect to the retention of the fibrous structure of VR. The temperature of activation with PO with or without a stabilisation step does not seem to significantly affect the morphology of the derived ACCs as shown in Fig. 3 and Fig. S7–S10 (ESI†). While there are some minor differences in morphology between series VRnP-*T* (Fig. 3 middle row and Fig. S9, ESI†) and VRcP-*T* (Fig. 3 bottom row and Fig. S10, ESI†), with the latter showing slightly higher retention of structural intgerety, there is not sufficient evidence to indicate major differences with respect to effects on morphology of PO-activated ACCs derived by using NH$_4$Cl stabilisation of VR *versus* carbonisation at 800 °C.

3.3.1 Porosity. The textural properties of the flexible ACCs are shown in Table 4, and the N$_2$ sorption isotherms from which they are derived, and pore size distribution (PSD) curves in Fig. 4. Further details of the method used to determine the surface area can be found in the ESI† (Sections S6 and S7). The N$_2$ isotherms show high uptake at low relative pressure for all ACC samples, indicating a high proportion of microporosity. However the isotherm for VRnP-750 is not strictly type I (see Fig. 4(e)), possessing a type H2(a) hysteresis loop which may indicate a complex hierarchy of pore sizes. The isotherms

also exhibit an increase in N$_2$ uptake as $\frac{P}{P_0}$ approaches 1, most evident for samples in series VRnzZ-*X-T* (Fig. 4(a)), indicating adsorption on the external surface.

For VRnzZ-*X-T* samples, the surface area is in the range of 598–1222 m^2 g^{-1} and is highest for sample VRnzZ-50-630. The pore volume is between 0.24 and 0.47 cm^3 g^{-1}, which gives very high surface area density (SAD, ratio of surface area to pore volume) of between 2315 and 2600 m^2 cm^{-3}. The high SAD is consistent with the high microporosity of the carbons with the proportion of microporosity ranging from 93 to 99% for surface area and 84 to 99% for pore volume. In comparison, the surface area of VRnP-*T* ACCs ranges from 993 to 1933 m^2 g^{-1} with pore volume of 0.40 to 0.80 cm^3 g^{-1}. This gives SAD of between 2416 to 2482 m^2 cm^{-3}, and equally high levels of microporosity (Table 4). The textural data in Table 4 suggests that a temperature of ~750 °C is most suitable for activation *via* this route as sample VRnP-750 has surface area and pore volume that is almost double that achieved at 800 and 900 °C but without loss of microporosity. A similar temperature effect, with optimal performance at 750 °C, is observed for VRcP-*T* samples. All VRcP-*T* samples have SAD above 2240 m^2 cm^{-3} except for VRcP-750 (1767 m^2 cm^{-3}), a trend that is also observed for the level of microporosity.

In terms of overall porosity (Table 4), samples activated using PO at 750 °C (VRnP-750 and VRcP-750) outperform samples activated with ZnCl$_2$, or those activated at other temperatures. Indeed, the A_{BET} and V_{sp} of these samples are approximately twice that of any other sample in this work. A similar effect is seen for total values of A_{NLDFT} and V_{NLDFT}, though less pronounced.§

---

§ This is perhaps due to the fact that these calculations only take into account porosity in pores smaller than 500 Å, *i.e.* excluding the external surface. Furthermore the NLDFT kernel used in this work accounts for surface heterogeneity, and the BET method is a poor method of determining surface area in microporous materialsi as it only accounts for adsorption of N$_2$ onto a single surface.[38–41] This may account for the fact that the range of values for A_{NLDFT} is smaller than that for A_{BET}. On the other hand, values for V_{NLDFT} and V_{sp} are similar, as the assumptions used in determination of V_{sp} do not exclude micropores.
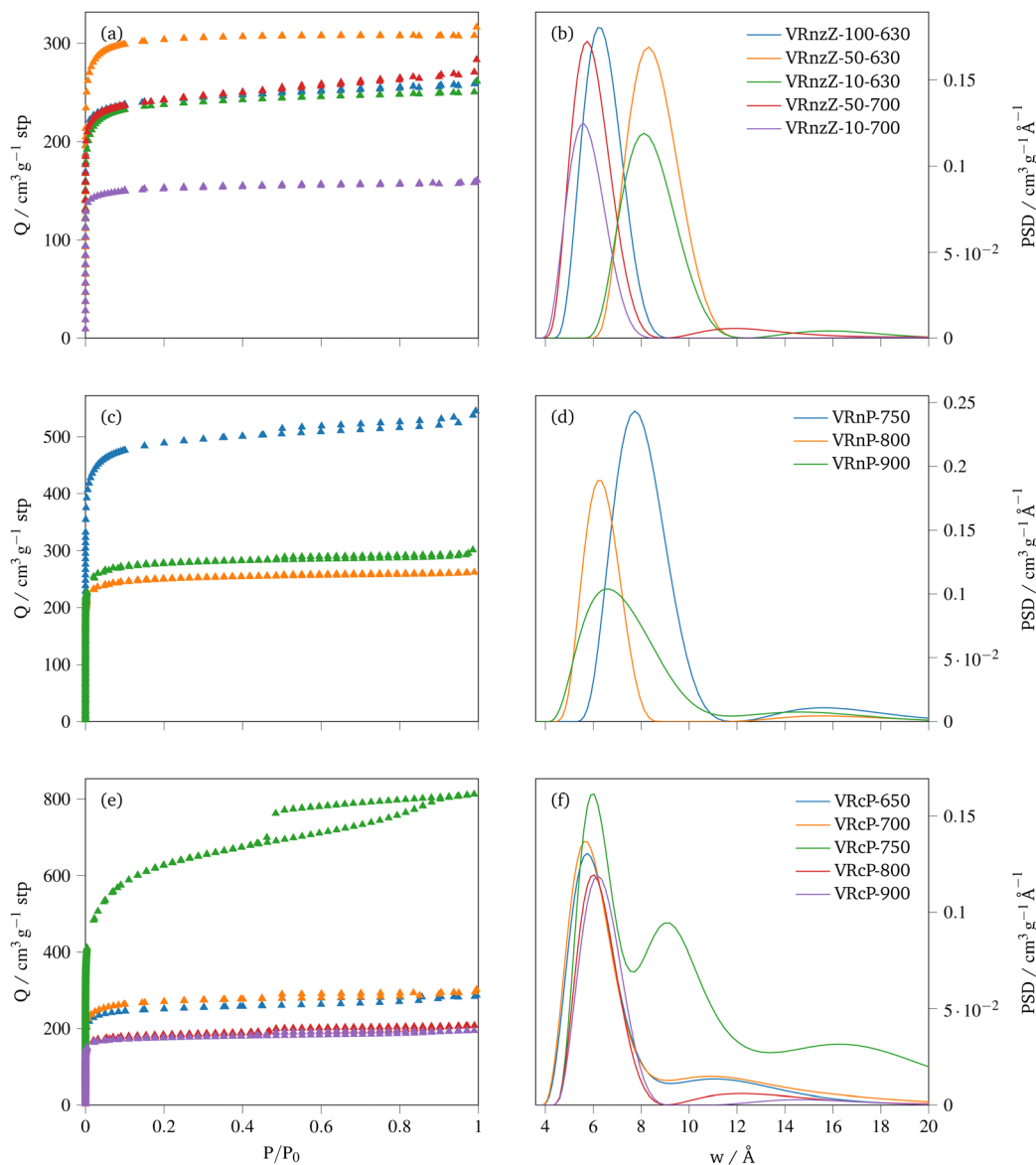
Fig. 4 N$_2$ isotherms for flexible ACCs (a), (c) and (e) and PSDs derived *via* fitting to the 2D-NLDFT heterogeneous surface kernel (b), (d) and (f) for sample series VRnzZ-*X-T* (top row), VRnP-*T* (middle row) and VRcP-*T* (bottom row).

The greater maximal porosity of PO-activated materials relative to those activated with ZnCl$_2$ is a result of the difference in their activation mechanisms, in that ZnCl$_2$ is limited in its ability to create pores by the availability of moieties present in the precursor which are susceptible to dehydration reactions. Indeed the relatively high heteroatom content of VRnzZ-*X-T* (see Table 2) samples is indicative of the fact that a relatively low proportion of moieties susceptible to dehydration reactions were in fact eliminated *via* dehydration. In the case of PO-activated samples, the maximisation of porosity at 750 °C can be attributed to an optimisation in the balance of mobility of K$^+$ ions with the effects of overactivation at high temperatures.

Most of the flexible ACC samples are almost entirely microporous - regardless of activating/stabilising reagents and conditions - according to t-plot calculations (at least 92 and

85% in terms of A_{BET} and V_{sp} respectively), the key outlier being VRcP-750 having approximately a third of its pore volume made up by pores of widths larger than 20 Å. Corresponding NLDFT-derived values of porosity were used to estimate porosity below 10 Å as this has been shown to be important for low pressure uptakes of both CO$_2$ and CH$_4$, and a similar trend is exhibited as in the classical measures of porosity; all samples except VRcP-750 have the majority of their porosity arising from pores of size <10 Å. This is also evident when comparing PSDs of the samples, as shown in Fig. 4(c), with VRcP-750 clearly exhibiting a broad, hierarchical PSD unlike the other samples - as can be expected due to the shape of the isotherm. The origin of the broad porosity in VRnP-750 relative to the narrow PSDs of the other VRnP-*T* ACCs is perhaps a result of activation at 750 °C facilitating oxidative porogenesis to occur, thus forming

supermicropores and mesopores. Regarding the VRcP-*T* series, it appears that 750 °C whilst facilitating creation of super-micropores and mesopores, is however, still not severe enough to lead to overactivation of VRc, which prevents the destruction of the aforementioned larger pores. Raising the activation temperature to ≥ 800 °C, however does seem to overactivate VRc.

Activation of NH$_4$Cl-stabilised VR at 750 °C (VRnP-750) appears to yield pores centred at 8 Å while activation at 800 and 900 °C generates smaller pores (Fig. 4(d)). This likely contributes to the overall high porosity for VRnP-750. Typically, pore sizes shift to larger values with increasing activation temperature which is the opposite of the trend seen for VRnP-*T*. To further explore this unusual trend, it is useful to look to variations in the elemental composition of the VRnP-*T* samples (see Table 3). VRnP-750 has a significantly higher O content (24 wt%) than the other two samples (both $\sim$16 wt%), indicating that reactions of porogen-derived compounds to remove oxygen-rich moieties are more extensive at higher temperatures during PO-activation of NH$_4$Cl-stabilised VR. On the other hand, for the samples derived *via* carbonisation followed by activation with PO (VRcP-*T* series), while the broad-ening in PSD follows the same trend as VRnP-*T* series, the oxygen content is at its minimum for the sample activated at 750 °C. This indicates that the stabilisation effects for which NH$_4$Cl has been employed in previous steps include limiting reactions of porogen with the aforementioned O-rich groups during pyrolysis, which in turn limits the porosity development achievable at higher temperatures, which is consistent with the data for VRnzZ-*X*-*T* series in Table 2. While referring to the variation O-content, it is important to note that while the 2D-NLDFT heterogeneous surface kernel does account for chemical heteroregeniety of the pore,[41] it may not account for the differences in O-content across different samples. Thus, the exact position of pore widths has a certain degree of uncertainty.

For samples derived by stabilisation with NH$_4$Cl and activation with ZnCl$_2$, there are only small variations in total porosity and indeed microporosity (Table 4). However, there appears to be a relationship between synthesis conditions and the pore size; samples VRnzZ-50-630 and VRnzZ-10-630 have PSD centred at 8 to 9 Å while all other ACCs in the series have have the the majority of pores with size ≤ 6 Å. It has previously been shown that increasing amount of ZnCl$_2$ during activation of biomass can lead to higher overall porosity, and shifting of micropore widths to higher values.[52,53] This can explain the larger pores for VRnzZ-50-630 and VRnzZ-10-630, but less so the apparent temperature-dependence of the PSD. As the size and distribution of pores formed by ZnCl$_2$ activation of the NH$_4$Cl-stabilised VR is known principally to be driven by dehydration around ZnCl$_2$ and its hydrates, it is possible that at 700 °C any water associated with the ZnCl$_2$ crystal structure is driven off before porogenesis occurs, thus yielding smaller pores.

As stated above, the aim of the present work was to simplify the preparation of ACCs. This has been successfully achieved as we have been able to prepare fully flexible, cloth-like ACCs *via* a much simpler route that negates the need for stabilisation and only requires carbonisation of VR followed by conventional activation with PO. The use of PO, as a milder activating agent rather than KOH, which is harsher, is key in achieving flexible ACCs. Our route simplifies the synthesis route (fewer steps, fewer reagents as only PO is needed), and lower energy use. In additon to the advantage of a simpler process, our routes yield ACCs with enhanced porosity with surface area and pore volume of up to 2226 m^2 g^{-1} and 1.26 cm^3 g^{-1}, respectively. These textural properties are higher than those previously achieved for current state-of-the-art ACCs prepared *via* more complicated synthesis routes.[20,23,25] This porosity also exceeds that of the commercially available VR-derived ACC, Calgon Zorflex (A_{BET} of up to 1300 m^2 g^{-1} and V_{sp} of up to 0.44 cm^3 g^{-1}),[54] as well as other commercial ACCs derived from other precursors (A_{BET} in range 600 to 1700 m^2 g^{-1} and V_{sp} in range 0.27 to 0.64 cm^3 g^{-1}).[13,14,15,16] In the next section we explore the gas (CH$_4$ and CO$_2$) uptake of the present ACCs and compare them to previous benchmark ACC materials.

3.3.2 Gas uptake capacity. The high microporosity of the flexible ACCs means that they are likely to be interesting for the storage of CO$_2$ and CH$_4$ as both gases are best stored in porous materials that possess micropores.[50,51,55] This is especially the case for the storage of CO$_2$ at low pressure (<1 bar), while storage of both gases at higher pressure (>20 bar) is also aided by the presence of mesopores.[50,51,56] In this regard, it is known that CO$_2$ uptake at low pressure is determined by the micro-porosity, with highly microporous materials excelling regard-less of total porosity. On the other hand high pressure CO$_2$ and CH$_4$ uptake is more dependent on the total porosity and rises with total surface area and pore volume. Given the comparable level of microporosity of the present flexible ACCs in each series, the trend in their gas uptake capacity will be mainly determined by the total porosity rather than any differences in PSD. For this reason, the discussion on gas uptake focusses on the ACCs from each series with the highest porosity, namely VRnzZ-50-630, VRnP-750 and VRcP-750. Furthermore, although the total porosity of VRnzZ-50-630 is lower than that of the other two samples, it is still of interest for low pressure CO$_2$ uptake due to pores centred around 8 Å as well as high N-content (Table 2).[5,56,57] Thus, samples VRnzZ-50-630, VRnP-750 and VRcP-750 are discussed below in terms of their CO$_2$ and CH$_4$ capacities. Nevertheless, CO$_2$ and CH$_4$ isotherms were also measured on some of the remaining VRnzZ-*X*-*T* samples, (Fig. S32 and S33, ESI†).

3.3.2.1 CO$_2$ capture. Excess isotherms for CO$_2$ uptake on the selected ACCs are shown in Fig. 5 with tabulated uptake values in Table 5. It is clear that the high overall porosity (Table 4 and Fig. 4) of VRcP-750 means it outcompetes the other two in terms of CO$_2$ capacity at high pressures, reaching 16.3 mmol g^{-1} at 40 bar, in line with previous reports.[5,57] It is apparent that the porosity and/or compositions of the other two samples show some benefit for low pressure CO$_2$ uptake as shown in Fig. 5(b). We have recently shown that at pressures below 10 bar, volume in pores of width less than 10 Å are highly associated with CO$_2$ uptake at 25 °C.[57] This serves to explain why VRnP-750 outperforms VRcP-750 at sufficiently low
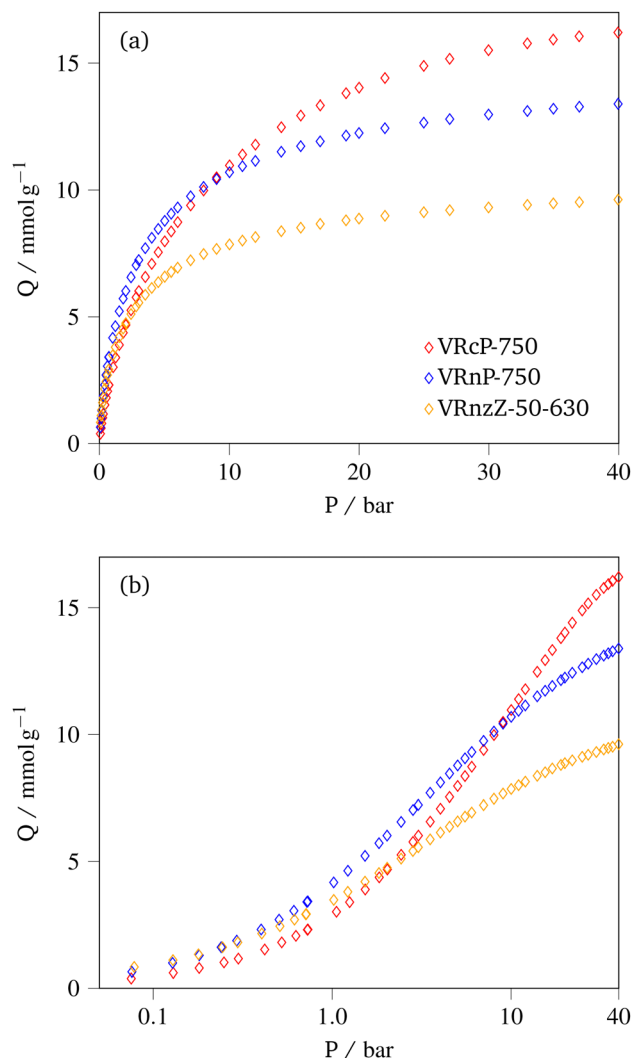
Fig. 5 Excess gravimetric CO_2 uptake isotherms measured at 25 °C up to 40 bar, with a linear (a) and logarithmic (b) pressure scale.

Table 5 Uptake of CO_2 for selected samples at application-relevant pressures, as well working capacity, W betewen 1 and 40 bar

| Sample | Q/mmol g^{-1} | | | | |
	0.15	1.0	20	40	W
VRcP-750	0.63	2.9	14.0	16.3	13.4
VRnP-750	1.1	4.1	12.3	13.3	9.2
VRnzZ-50-630	1.2	3.5	8.9	9.5	6.0

Furthermore, a flexible ACC just as suited for high pressure (20 bar) uptake can be achieved by eliminating the stabilisation step in favour of a carbonisation step. This further reduces the number of reagents needed in the synthesis of ACC from VR. Attia *et al.* attributed their material's high CO_2 capacity at 20 bar to a combination of high surface area and N-doping (up to 10 wt%).[20] However, considering sample VRcP-750 contains no N and has similar porosity to the best performing sample in the aformentioned work, while achieving the same excess CO_2 uptake, it can be assumed that porosity is likely the determining factor for CO_2 capture at 20 bar.

3.3.2.2 CH$_4$ storage. CH_4 uptake isotherms for the three samples are shown in Fig. 6 and the uptake at various pressures is given in Table 6. It should be noted that for VRcP-750 and VRnP-750 there are apparent uptake maxima in the isotherms at approximately 61 and 90 bar respectively (see Fig. 6(a)). This is a phenomenon observed commonly in high pressure adsorption of supercritical fluids, and indicates that the density of bulk or free CH_4 is increasing more quickly with pressure than the density of adsorbed CH_4 (pore density).[43,59–61] The fact that this maximum occurs at a higher pressure for VRnP-750 than for VRcP-750, and is not visible for VRnzZ-50-630 indicates the the rate of pressure-dependent change in pore density of methane (ρ_{ads}) at a given pressure varies in the order VRcP-750 < VRnP-750 < VRnzZ-50-630. For VRnzZ-50-630 the maximum likely exists *ca.* 100 bar where it has been frequently observed on shale samples.[43,62,63] The differences in ρ_{ads} between these three samples is probably best ascribed to differences in pore structure, as supercritical adsorption only takes place *via* micropore adsorption followed by monolayer formation in mesopores.[43] ρ_{ads} is thus higher in samples that are proportionally more microporous, whereas adsorption in mesopores hardly contributes to the adsorbed gas density.

Total uptake, Q_t at high pressure is the more relevant parameter for CH_4 storage applications. While VRnP-750 noticeably outperforms VRcP-750 in terms of excess CH_4 storage at pressures under 20 bar, the latter exceeds the former in terms of high pressure total CH_4 uptaake. This is because of the high overall pore volume of VRcP-750, which outweighs its relatively low porosity in the width range 8.0 to 15 Å. Similarly, the significantly lower capacity of VRnzZ-50-630 can be attributed to a much lower pore volume, only becoming competitive with the PO-activated samples at very low pressures. Unlike for CO_2 capture, the composition of the samples plays little role in improving CH_4 uptake thus the relatively high low-pressure uptake must be solely attributed to porosity. In a similar

pressures, having pore volume of 0.62 cm^3 g^{-1} as compared with 0.50 cm^3 g^{-1} in this width range (see Table 4). At very low pressures ($\sim$0.10 bar), N-rich (6.1 wt%) VRnzZ-50-630 becomes competitive compared to the other two samples despite having approximately half the overall porosity. While the effects of N-doping *versus* pore size on CO_2 uptake remain a subject of debate,[8,58] recent work by Burrow *et al.* suggests that the N-content becomes more important at very low pressures[56] - a phenomenon which appears to be confirmed by the results shown here.

Until now, the best ambient temperature CO_2 uptakes in ACCs have been reported by Attia and co-workers *via* the activation of a ZnCl$_2$/NH$_4$Cl-stabilised VR-polypyrrole composite with KOH, which achieved CO_2 uptake capacities of 4.2 and 14.3 mmol g^{-1} at 1.0 and 20 bar respectively.[20] Our methods yield flexible ACCs with similar uptakes but eliminate the need for the formation of the polypyrrole composite, as well as the necessity of using ZnCl$_2$ and/or NH$_4$Cl. Additionally, our simpler synthesis routes use the milder PO as activating agent.
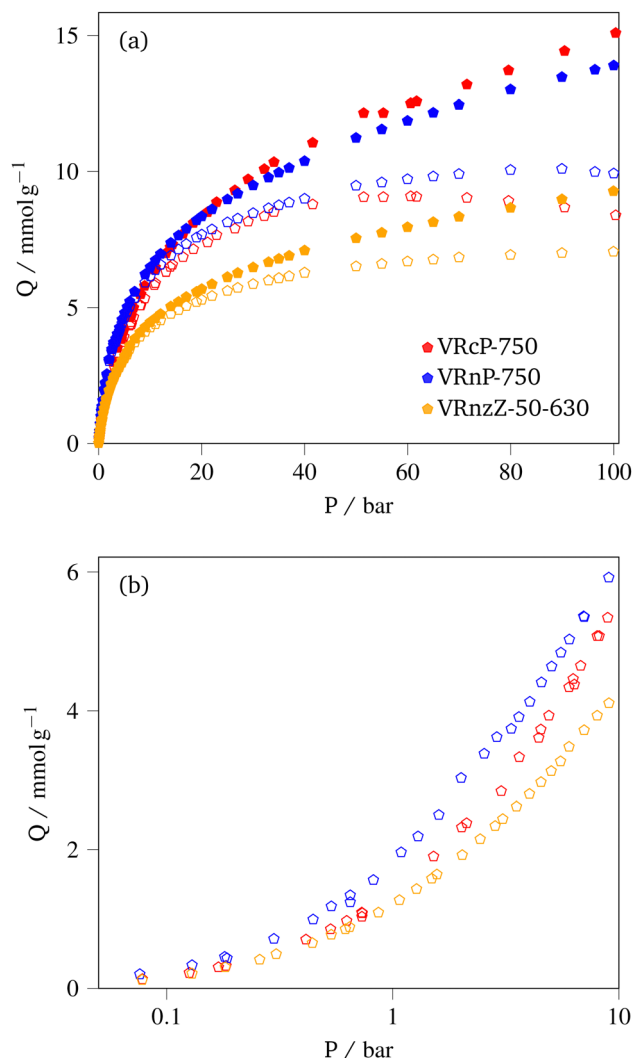
Fig. 6 Gravimetric CH_4 uptake isotherms measured at 25 °C up to 100 bar, with a linear pressure scale (a) and up to 10 bar with a logarithmic pressure scale (b). Filled symbols indicate total uptake and empty symbols are excess. Total uptake is not included in (b) as total uptakes are only relevant at high pressures.

Table 6 Excess and total (in brackets, where relevant) uptake of CH_4 for selected samples at various pressures, column 'max' uses the peak of the isotherm (if exists) for excess, and 100 bar uptake for total

Sample	Q/mmol g^{-1}							
	1.0	20		35		Max	
VRcP-750	1.3	7.3	(8.3)	8.2	(10.4)	8.9	(14.8)
VRnP-750	1.9	7.7	(8.3)	8.8	(10.0)	10.2	(13.8)
VRnzZ-50-630	1.2	5.3	(5.6)	6.1	(6.8)	7.1	(9.2)

manner to CO_2 uptake, the PO-activated samples achieve similar high and low pressure CH_4 uptakes to those reported by Attia and co-workers,[20] despite our much simpler synthetic methods. Indeed, stabilisation of VR can be completely foregone to achieve greater total capacity than found previously, at 20 bar.

4 Conclusions

The development of flexible nanoporous and high surface-area carbon materials may show promise for applications involving the adsorption of small molecules. However, thus far the typical synthesis from viscose rayon (VR) is complex and unsustainable, requiring so-called stabilising reagents ($ZnCl_2$ and NH_4Cl) as well as corrosive activating agents such as KOH, and in some cases the formation of composites with VR prior to activation. In this study, a series of mechanically stable and flexible activated carbon cloths (ACCs) were prepared with the view to iteratively eliminate many of the steps and reagents used in previous studies. We found that the use of toxic $ZnCl_2$ in the stabilisation step hinders the development of the porosity important for CO_2 capture and CH_4 storage. Furthermore, KOH can be replaced as activating agent by potassium oxalate (PO) to yield highly microporous carbons, and has the advantage of not risking compromising flexibility of the ACC product. Upon optimisation of reaction conditions, a flexible ACC was achieved with impressive surface area and pore volume of 1933 m^2 g^{-1} and 0.80 cm^3 g^{-1} respectively of which 95% is in micropores. This resulted in excellent CH_4 uptake at 25 °C of 1.9 and 9.3 mmol g^{-1} at 1.0 and 35 bar respectively. Furthermore, the material may be interesting for ambient CO_2 capture as an uptake of 4.2 mmol g^{-1} at 25 °C and 1 bar was achieved. Synthesis protocols can be further simplified by elimination of the stabilisation step altogether in favour of a short pyrolysis step that, surprisingly, further increased the porosity. The resulting PO-activated flexible ACC has surface area of 2226 m^2 g^{-1} and pore volume of 1.26 cm^3 g^{-1}. However, approximately a third of this porosity is in mesopores, resulting in a material suited for high pressure CO_2 capture applications with uptake of 16.3 mmol g^{-1} at ambient temperature and 40 bar. The porosities and gravimetric gas uptake capacities found here are comparable with those reported previously for ACCs which are derived through far more complex procedures.

Author contributions

Thria Alkhaldi: conceptualization, methodology, formal analysis, investigation, writing – review & editing. L. Scott Blankenship: writing – original draft, formal analysis, visualization, writing – review & editing, validation. Robert Mokaya: conceptualisation, writing – review & editing, supervision, funding acquisition, resources.

Conflicts of interest

There are no conflicts to declare.

Acknowledgements

References

1 D. Lozano-Castello, J. A. Monge, M. Lillo, D. Amoros and A. Solano, *Fuel*, 2002, **81**, 1777–1803.

2 B. M. Babic, S. K. Milonjic, M. J. Polovina and B. V. K. Kaludierovič, *Carbon*, 1999, **37**, 477–481.

3 A. Huidobro, A. Pastor and F. Rodrıguez-Reinoso, *Carbon*, 2001, **39**, 389–398.

4 L. S. Blankenship and R. Mokaya, *Mater. Adv.*, 2022, **3**, 1905–1930.

5 V. Presser, J. McDonough, S. H. Yeon and Y. Gogotsi, *Energy Environ. Sci.*, 2011, **4**, 3059–3066.

6 M. Cox and R. Mokaya, *Sustainable Energy Fuels*, 2017, **1**, 1414–1424.

7 K. R. Matranga, A. Stella, A. L. Myers and E. D. Glandt, *Sep. Sci. Technol.*, 1992, **27**, 1825–1836.

8 B. Adeniran and R. Mokaya, *Chem. Mater.*, 2016, **28**, 994–1001.

9 S. Reljic, E. Jardim, C. Cuadrado-Collados, M. Bayona, M. Martinez-Escandell, J. Silvestre-Albero and F. Rodríguez-Reinoso, *Porous Materials: Theory and Its Application for Environmental Remediation*, 2021, vol. 139.

10 S. Biloe, V. Goetz and A. Guillot, *Carbon*, 2002, **40**, 1295–1308.

11 E. Frank, L. M. Steudle, D. Ingildeev, J. M. Spörl and M. R. Buchmeiser, *Angew. Chem., Int. Ed.*, 2014, **53**, 5262–5298.

12 A. G. Dumanlı and A. H. Windle, *J. Mater. Sci.*, 2012, **47**, 4236–4250.

13 N. Kostoglou, C. Koczwara, C. Prehal, V. Terziyska, B. Babic, B. Matovic, G. Constantinides, C. Tampaxis, G. Charalambopoulou and T. Steriotis, *et al.*, *Nano Energy*, 2017, **40**, 49–64.

14 J. V. Nabais, T. Canário, P. Carrott and M. R. Carrott, *J. Porous Mater.*, 2007, **14**, 181–190.

15 C. Kim, P. Srimuk, J. Lee, S. Fleischmann, M. Aslan and V. Presser, *Carbon*, 2017, **122**, 329–335.

16 M. E. Ramos, P. R. Bonelli, A. L. Cukierman, M. R. Carrott and P. Carrott, *J. Hazard. Mater.*, 2010, **177**, 175–182.

17 P. Morgan, *Carbon Fibers and Their Composites*, CRC press, 2005.

18 J.-B. Donnet and R. C. Bansal, *Carbon Fibers*, CRC Press, 1998.

19 J. Hearle, *J. Polym. Sci.*, 1958, **28**, 432–435.

20 N. F. Attia, M. Jung, J. Park, H. Jang, K. Lee and H. Oh, *Chem. Eng. J.*, 2020, **379**, 122367.

21 N. Kostoglou, C. Koczwara, C. Prehal, V. Terziyska, B. Babic, B. Matovic, G. Constantinides, C. Tampaxis, G. Charalambopoulou, T. Steriotis, S. Hinder, M. Baker, K. Polychronopoulou, C. Doumanidis, O. Paris, C. Mitterer and C. Rebholz, *Nano Energy*, 2017, **40**, 49–64.

22 NEUROtiker, Structure of cellulose (chain conformation), 2007, **https://upload.wikimedia.org/wikipedia/commons/0/07/Cellulose_Sessel.svg**.

23 G. Rodríguez-Blanco, L. Giraldo and J. C. Moreno-Piraján, *Appl. Surf. Sci.*, 2010, **256**, 5221–5225.

24 X. Huang, *Materials*, 2009, **2**, 2369–2403.

25 M. Jung, J. Park, S. Y. Cho, S. E. Elashery, N. F. Attia and H. Oh, *Surf. Interfaces*, 2021, **23**, 100960.

26 P. E. Hock and M. A. A. Zaini, *Acta Chim. Slovaca*, 2018, **11**, 99–106.

27 M. A. A. Zaini and M. S. M. Shaid, *Hung. J. Ind. Chem.*, 2017, **44**, 129–133.

28 F. Suárez-García, A. Martínez-Alonso and J. M. D. Tascón, *Carbon*, 2004, **42**, 1419–1426.

29 M. Sevilla and R. Mokaya, *Energy Environ. Sci.*, 2014, **7**, 1250–1280.

30 L. S. Blankenship, N. Balahmar and R. Mokaya, *Nat. Commun.*, 2017, **8**, 1–12.

31 N. Balahmar and R. Mokaya, *J. Mater. Chem. A*, 2019, **7**, 17466–17479.

32 M. Sevilla, R. Mokaya and A. B. Fuertes, *Energy Environ. Sci.*, 2011, **4**, 2930–2936.

33 M. Sevilla, A. S. M. Al-Jumialy, A. B. Fuertes and R. Mokaya, *ACS Appl. Mater. Interfaces*, 2018, **10**, 1623–1633.

34 A. Altwala and R. Mokaya, *RSC Adv.*, 2022, **12**, 20080–20087.

35 M. Sevilla, G. A. Ferrero and A. B. Fuertes, *Carbon*, 2017, **114**, 50–58.

36 P. T. Williams and A. R. Reed, *J. Anal. Appl. Pyrolysis*, 2004, **71**, 971–986.

37 M. A. A. Zaini, T. W. Meng, M. J. Kamaruddin, S. H. M. Setapar and M. A. C. Yunus, *Sains Malays.*, 2014, **43**, 1421–1428.

38 J. Rouquerol, P. Llewellyn and F. Rouquerol, *Stud. Surf. Sci. Catal.*, 2007, 49–56.

39 J. W. Osterrieth, J. Rampersad, D. Madden, N. Rampal, L. Skoric, B. Connolly, M. D. Allendorf, V. Stavila, J. L. Snider and R. Ameloot, *et al.*, *Adv. Mater.*, 2022, 2201502.

40 J. Jagiello, *Langmuir*, 1994, **10**, 2778–2785.

41 J. Jagiello and J. P. Olivier, *Carbon*, 2013, **55**, 70–80.

42 D. Do and H. Do, *Carbon*, 2003, **41**, 1777–1791.

43 T. F. Rexer, M. J. Benham, A. C. Aplin and K. M. Thomas, *Energy Fuels*, 2013, **27**, 3099–3109.

44 I. H. Bell, J. Wronski, S. Quoilin and V. Lemort, *Ind. Eng. Chem. Res.*, 2014, **53**, 2498–2508.

45 Z. Yang, Y. Xia, X. Sun and R. Mokaya, *J. Phys. Chem. B*, 2006, **110**, 18424–18431.

46 J. Singh, S. Basu and H. Bhunia, *J. Taiwan Inst. Chem. Eng.*, 2019, **102**, 438–447.

47 Y. Li, S. Wang, B. Wang, Y. Wang and J. Wei, *Nanomaterials*, 2020, **10**, 174.

48 E. Fuente, R. Gil, R. Giron, M. Lillo-Ródenas, M. Montes-Moran, M. Martin and A. Linares-Solano, *Carbon*, 2010, **48**, 1032–1037.

49 N. Tsubouchi, M. Nishio and Y. Mochizuki, *Appl. Surf. Sci.*, 2016, **371**, 301–306.

50 A. Altwala and R. Mokaya, *Energy Environ. Sci.*, 2020, **13**, 2967–2978.

51 A. M. Aljumialy and R. Mokaya, *Mater. Adv.*, 2020, **1**, 3267–3280.

52 Q. Qian, M. Machida, M. Aikawa and H. Tatsumoto, *J. Mater. Cycles Waste Manage.*, 2008, **10**, 53–61.

53 F. Caturla, M. Molina-Sabio and F. Rodriguez-Reinoso, *Carbon*, 1991, **29**, 999–1007.

54 R. Kaiser, A. Kulczyk, D. Rich, R. J. Willey, J. Minicucci and B. MacIver, *Ind. Eng. Chem. Res.*, 2007, **46**, 6126–6132.

55 E. A. Hirst, A. Taylor and R. Mokaya, *J. Mater. Chem. A*, 2018, **6**, 12393–12403.

56 J. N. Burrow, J. E. Eichler, Y. Wang, D. C. Calabro and C. B. Mullins, *J. Mater. Chem. A*, 2022, **10**, 24649–24661.

57 L. S. Blankenship, N. Albeladi, T. Alkhaldi, A. Madkhali and R. Mokaya, *Energy Adv.*, 2022, **1**, 1009–1020.

58 M. Sevilla, J. B. Parra and A. B. Fuertes, *ACS Appl. Mater. Interfaces*, 2013, **5**, 6360–6368.

59 A. L. Myers and P. A. Monson, *Adsorption*, 2014, **20**, 591–622.

60 D. Do, H. Do, C. Fan and D. Nicholson, *Langmuir*, 2010, **26**, 4796–4806.

61 S. Zhou, H. Xue, Y. Ning, W. Guo and Q. Zhang, *Fuel*, 2018, **211**, 140–148.

62 X. Tang, N. Ripepi, N. P. Stadie, L. Yu and M. R. Hall, *Fuel*, 2016, **185**, 10–17.

63 H. Tian, T. Li, T. Zhang and X. Xiao, *Int. J. Coal Geol.*, 2016, **156**, 36–49.